Current Microbiology (2021) 78:3936–3944
https://doi.org/10.1007/s00284-021-02654-y

Mechanism Underlying the Role of LuxR Family Transcriptional Regulator *abaR* in Biofilm Formation by *Acinetobacter baumannii*

Xu Sun[1] · Jun Xiang[1]

Received: 12 January 2021 / Accepted: 2 September 2021 / Published online: 14 September 2021

Abstract
Our study attempted to explore the mechanism underlying the role of LuxR family transcriptional regulator *abaR* in biofilm formation by *Acinetobacter baumannii.* The *abaR* gene was knocked out in ATCC 17978 strain using homologous recombination method. The growth curve and biofilm formation were measured in the wild type and *abaR* gene knockdown strains. Transcriptome sequencing was performed in the wild type and *abaR* gene knockdown strains following 8 h of culture. The growth curve in the *abaR* gene knockdown strain was similar to that of the wild-type strain. Biofilm formation significantly declined in the *abaR* gene knockdown strain at 8 and 48 h after culture. A total of 137 differentially expressed genes (DEGs) were obtained including 20 downregulated DEGs and 117 upregulated DEGs. Genes with differential expression were closely related to viral procapsid maturation (GO:0046797), acetoin catabolism (GO:0045150), carbon metabolism (ko01200), and the glycolysis/gluconeogenesis (ko00010)-related pathways. The results of the eight verified expression DEGs were consistent with the results predicted by bioinformatics. *AbaR* gene knockdown significantly affected biofilm formation by *A. baumannii* ATCC 17978 strain. The glycolysis/gluconeogenesis pathways were significantly dysregulated and induced by *abaR* gene knockdown in *A. baumannii.*

Introduction

Acinetobacter baumannii is a Gram-negative coccobacillus which is troublesome pathogen in hospitalized patients globally. *A. baumannii* has emerged as a major challenge in infected patients because of its multiple drug resistance [1, pp. 939–951]. Recent data show that *A. baumannii* is one of the top four most common pathogens isolated in the hospital environment between 2005 and 2017 in China [2, pp. S128–S134]. In global intensive care units (ICUs), the infection rate of *A.* baumannii accounts for 20% of the total number of infections [3, pp. 25–36]. The resistance profile of *Acinetobacter* spp. indicates that the resistance rate against the five commonly used antimicrobials, except amikacin, is increasing. The resistance rate of *A. baumannii* against carbapenems varied from 18 to 25% in different provinces of China [2, pp. S128–S134]. *A. baumannii* can cause a variety of nosocomial infections, most of which involve the respiratory tract and some involve skin wound infections and bacteremia [4]. This is corroborated by the report that *A. baumannii* is an increasing threat in burn centers because of its high multidrug resistance based on clinical data obtained from a comprehensive hospital covering 2007–2013 and the CHINET (the surveillance system for bacterial epidemiology and resistance in China) data [5, pp. 1718–1719].

Considerable attention has been focused on exploring the mechanism of drug resistance in *A. baumannii* in clinical settings [6]. One of the major factors associated with bacterial resistance to antimicrobials is the ability to form biofilms. Previous studies have shown that strains that can form biofilms are more resistant to antibiotics than strains that cannot [7]. Recent evidence shows that biofilm formation is closely related to drug resistance and virulence in *A. baumannii* [8, pp. 119–127]. It is reported that the biofilm-forming ability of *A. baumannii* in a solid–liquid interface is approximately three times higher than that of other *Acinetobacter* species [9, pp. 1–4]. *A.* baumannii can rapidly produce biofilms while forming antibiotic resistance, and the level of biofilm-specific resistance can vary according to the induction response of the biofilm population and the action mechanism of antibiotics [10, p. 817]. Cold plasma technology, as a new tool for purification of biofilm-contaminated surfaces, has received more and more clinical attention. The

✉ Jun Xiang
13801789791@163.com

[1] Department of Burn, Ruijin Hospital Affiliated to Shanghai Jiao Tong University School of Medicine, Shanghai, China

increase in the amount of *A*. baumannii biofilm could reduce the antibacterial effect of cold plasma, thereby improving its tolerance to cold plasma exposure [11, pp. 344–349]. The biofilm formation characteristics of *A*. baumannii are related to the expression of genes. The genes that have been reported to be associated with the formation of *A*. baumannii biofilm include *csu* locus, *bap*, *abaI*, *adeFGH*, and *ompA* [7]. *csuE* encodes a fimbriae assembly system, and the formation of fimbriae is an important step in the formation of biofilm on non-living surfaces [12, pp. 3473–3484]. *Bap* can support the development of mature biofilm structures [13, pp. 1036–1044]. The mutation of *abaI* will cause the failure of the acyl-homoserine lactone signals to be generated and further damage the maturation of the biofilm [14, pp. 951–957]. *adeFGH* is involved in the synthesis and transport of autoinducer molecules during the formation of biofilms [15, pp. 4817–25]. *ompA* encodes a porin protein involved in the formation of biofilms [16, pp. 3150–3160]. Previous reports have implicated the *abaR* gene in *A. baumannii* biofilm formation and disruption of *abaR* expression is associated with a decline in biofilm formation [17, pp. 1802–1805; 18, pp. 200–205; 19, pp. 1339–1346]. Although there have been advances in exploring the mechanism underlying biofilm formation, the role of abaR at the transcriptome level has not been clarified completely.

Therefore, in this study, we aimed to determine the role of *abaR* in *A. baumannii* biofilm formation through *abaR* knockdown and explore the mechanism regulated by *abaR* expression using high-throughput transcriptional sequencing.

Materials and Methods

Bacterial Strains and *abaR* Gene Knockouts

A. baumannii ATCC 17978 strain was obtained from Shanghai Santa Biotechnology Co. Ltd., Shanghai, China. The ATCC 17978 strain was cultured in Luria–Bertani (LB) medium at 37 °C overnight. The *abaR* gene knockdown was performed using homologous recombination method [20, pp. 3743–3751]. A recombinant DNA fragment (ΔabaR::Kn) consisting of kanamycin resistance gene (Kn) sequences (obtained from pKD4 plasmid using PCR) and the upper and lower homologous recombination arms for *abaR* gene (amplified from ATCC17978 genome using PCR) were obtained using splicing PCR technology. ΔabaR::Kn target fragments were amplified by transferring them into pUC19 vector and tested by PCR analysis. The primers used are listed in Supplementary Table 1. Next, ΔabaR::Kn sequences were linked to pCVD442 vector and transferred to *Escherichia coli* β2155 by electrotransformation. Conjugation between ATCC17978 strain and the *E. coli* was performed and the knockdown ATCC17978 strains were selected for kanamycin resistance [21, pp. 71–76].

Construction of Complementary Strains

To complement the knockout mutant, the target gene *abaR* was amplified from the cDNA of ATCC17978 strain, and the amplification product was cloned into the vector pBAD33-TC^R to construct a pBAD33-TC^R-*abaR*. The vector pBAD33-TC^R has the origin of replication ori amplified on the pWH1266 plasmid and the tetracycline resistance gene; so, this plasmid can be amplified in *A. baumannii*. Then, pBAD33-TC^R-*abaR* was transformed to *E. coli* competent cells DH5α. The plasmids that were positive after tetracycline screening were sequenced. Then, the plasmids with correct sequencing results were transferred to *E. coli* β2163 competent cells and the positive clone *E. coli* β2163-[pBAD33-TC^R-*abaR*] was screened. Finally, *E. coli* β2163-[pBAD33-TC^R-*abaR*] was transformed into knockdown ATCC17978 strains using electrotransformation method [22, pp. 162–168] and the recombinant clones were screened out, followed by PCR verification, and PCR products are sequenced for sequence confirmation (Supplementary Fig. 1). The primers used in this section were listed in Supplementary Table 2.

Growth Curve Analysis

ATCC 17978 and *abaR* knockdown strains at 1×10^8 CFU/mL were maintained in fresh LB media at 37 °C for consecutive 18 h. The optical density (OD) of cultured strains in each group was evaluated for each hour using a Microplate reader (Bio-Rad, Hercules, CA, USA). There were three repeats in each group.

Biofilm Formation Analysis

Next, 200 μL of strain cultures (1×10^8 CFU/mL) was seeded onto each well of a 96-well plate. After culturing for 8, 24, and 48 h, the cultures were washed thrice with 200 μL PBS. Next, the cultures were fixed in methanol for 15 min followed by staining with 0.2% crystal violet solution for 20 min. After washing, 200 μL of 33% glacial acetic acid was added to each well and then, OD values were measured using a Microplate reader.

RNA Sequencing

After culturing for 8 h, ATCC17978 and *abaR* knockdown strains were collected for further analysis. Total RNA of the cultures in the two groups were isolated using mirVana miRNA isolation kit (Ambion) following the manufacturer's protocols, separately [23, p. e72968]. Because the vast

majority of RNA in bacteria is rRNA, rRNA was obtained using Ribo-Zero Magnetic Kit (MRZB12424, Illumina, CA, USA) and removed, following which the mRNAs were broken into fragments as templates for cDNA synthesis [24]. An RNA library was constructed using PCR analysis. The quality and size of the DNA fragments were evaluated using Agilent 2100 Bioanalyzer. The whole transcriptome was then sequenced based on the Illumina platform.

Data Processing

The raw data were downloaded and quality control was performed, using Trimmomatic software, including removing adaptor and low-quality reads. Clean reads were then mapped to reference genome using Rockhooper2 software. The gene expression level was measured based on the number of reads mapped to the genome and exome according to the reads per kilobase per million mapped reads (RPKM) method. The formula is provided in Eq. (1) as follows:

$$\mathrm{RPKM} = \frac{\text{Total exon reads}}{\text{Mapped reads(millions)} \times \text{exon length(KB)}}. \quad (1)$$

Differentially Expressed Gene Analysis

The gene counts were normalized using DESeq software to produce the significant genes with differential expression between the *abaR* knockdown ATCC 17978 and wild-type ATCC 17978 strains. The fold change (FC) of gene expression was calculated and negative binomial distribution test was applied to evaluate the significance of the differences in gene reads between two samples. The log|FC|> 1.5 and P value < 0.05 were set as the cutoff values.

Function Enrichment Analysis

The Gene Ontology (GO) project provides the possibility of biological function annotation of genes of interest [25, pp. D322–D326]. The differentially expressed genes were subjected to GO function analysis and the significant P values were tested using the hypergeometric distribution test. GO terms with P values < 0.05 were considered significant.

Pathway Enrichment Analysis

The Kyoto Encyclopedia of Genes and Genomes (KEGG) (http://www.genome.ad.jp/kegg/) is a pathway-related database [26, pp. 91–100]. KEGG pathway enrichment analysis was performed to explore the pathways involved in differentially expressed genes using the DAVID online tool. The enrichment P values were calculated using the hypergeometric distribution test. A P value < 0.05 was considered the cutoff value.

Real-Time Reverse Transcription-PCR Verification

RT-PCR was carried out to determine the relative expression of some DEGs. Total RNA was isolated from wild-type strains, mutant strains, and complementary strains after 8 h of culture. The concentration of RNA was detected using NanoDrop 2000. RNA was reverse-transcribed to cDNA using TransScript All-in-One First-Strand cDNA Synthesis SuperMIX for qPCR kit. PerfectStartTM Green qPCR SuperMix kit and LightCycler® 480 system were used together to perform RT-PCR. All assays were performed in triplicate. The relative expression levels of RNAs were calculated using the $2^{-\Delta\Delta Ct}$ method. 16 s was set as internal control. The primer sequences are listed in Supplementary Table 3.

Statistical Analysis

The data for strain growth and biofilm formation are expressed as mean ± standard deviation (SD). Multiple group comparison was performed using one-way ANOVA analysis and the difference between two groups was analyzed using the LSD test. $P < 0.05$ was considered significant.

Deposit the RNA-Seq Data

The raw sequencing data were deposited in the National Center for Biotechnology Information (NCBI) Sequence ReadArchive (SRA) database under accession number PRJNA720897.

Results

Effective *abaR* Gene Knockouts in ATCC 17978 Strain

PCR analysis of a recombinant DNA fragment (ΔabaR::Kn) showed that the size of the target sequence was 3029 bp (Fig. 1A). Next, the knockdown ATCC17978 strain was selected for kanamycin resistance. The PCR amplification of the target fragment was about 3300 bp, which indicated that the *abaR* gene sequence was successfully replaced by ΔabaR::Kn target fragment (Fig. 1B).

Growth Curve of ATCC 17978 Strain and *abaR* Knockdown Strain

The strain growth curve in Fig. 2 showed that the OD values for the ATCC 17978 strain were slightly higher than the *abaR* knockdown strain at 2, 3, and 4 h of culture. No

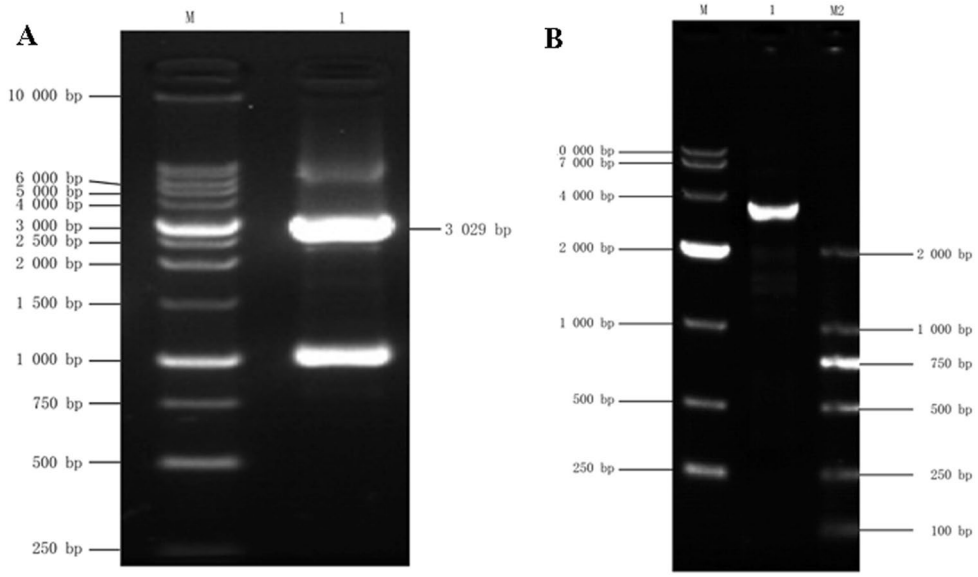

Fig. 1 Size of the target fragments (ΔabaR::Kn) by PCR analysis (**a**) and the *abaR* gene knockdown determined by PCR analysis (**b**). **a**: M, marker; 1, target (ΔabaR::Kn) fragment (size: 3029 bp). **b**: M, DL10000 marker; M2, DL2000 marker; 1, tested fragment after abaR gene knockdown (size: 3300 bp)

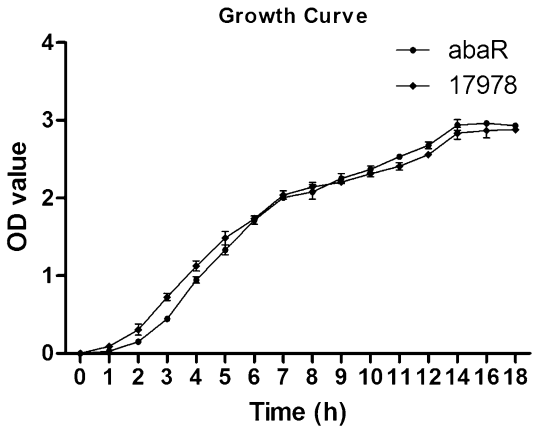

Fig. 2 Growth curve for ATCC 17978 strain after abaR gene knockdown, compared with wide-type strain. The OD value of strains after abaR gene knockdown was observed at 0–18 h of culture. There were three repeats in each group

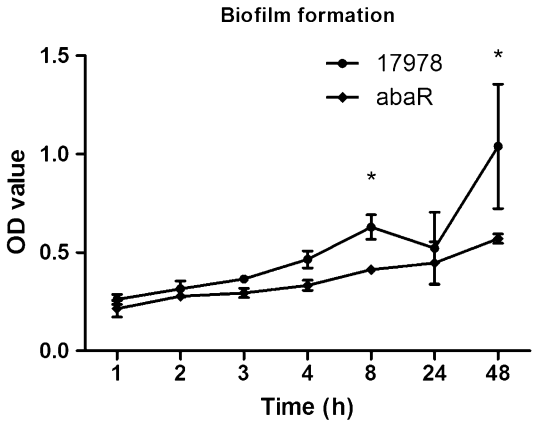

Fig. 3 Biofilm formation of ATCC 17978 strain after *abaR* gene knockdown, compared with wide-type strain. *$P < 0.05$, compared with wide-type ATCC 17978 strain. There were three repeats in each group

significant differences were observed in the OD values of the two strain groups from 5 to 12 h of culture. All strains entered the plateau stage after 14 h of culture. ATCC17978 entered the exponential growth stage during 3–4 h of culture in vitro and entered the plateau stage at 14 h, which was similar to the growth curve of the *abaR* knockdown strain.

Biofilm Formation Analysis

As shown in Fig. 3, biofilm formation by the ATCC 17978 strain increased in a time-dependent manner and peaked at 48 h of culture. However, there were no significant changes in the biofilm-forming ability of *abaR* knockdown strains during 0–8 h of culture. The biofilm-forming ability in the wild type and *abaR* knockdown strains was similar at 0–4 h of culture. At 8, 24, and 48 h after strain culture, the OD value of ATCC 17978 was 0.63 ± 0.06, 0.522 ± 0.18, and 1.04 ± 0.32, respectively. After *abaR* gene knockdown, the OD value was 0.41 ± 0.20, 0.45 ± 0.11, and 0.57 ± 0.02 at 8, 24, and 48 h, respectively. There were significant differences in OD values at 8 and 48 h of culture between the groups (all P values < 0.05), indicating that biofilm formation significantly declined in the ATCC 17978 strain after *abaR* knockdown.

Identification of Differentially Expressed Genes

With the cutoff value of $\log|FC| > 1.5$ and P value < 0.05, a total of 137 differentially expressed genes (DEGs) were obtained between the wild type and *abaR* knockdown

strains, including 20 downregulated genes and 117 upregulated genes (Supplementary Table 4). The volcano plot of genes with differential expression is shown in Fig. 4.

Significant Biological Processes and Pathways for Differentially Expressed Genes

GO analysis was performed for all the genes with differential expression. A total of 79 GO terms were enriched by differentially expressed genes, among which 58 GO terms were significantly enriched with $P < 0.05$. The differentially expressed genes were closely related to acetoin catabolic process (GO:0045150, BP), glycolytic process (GO:0006096, BP), tartrate dehydrogenase activity (GO:0009027, MF), and viral capsid (GO:0019028, CC). A total of 22 pathways were significantly enriched and the top 15 significant pathways are listed in Table 1. The results showed that pathways such as glycolysis/gluconeogenesis (ko00010), pyruvate metabolism (ko00620), and glucagon signaling pathway (ko04922) were dysregulated in *abaR* knockdown strains compared with the wild-type ATCC 17978.

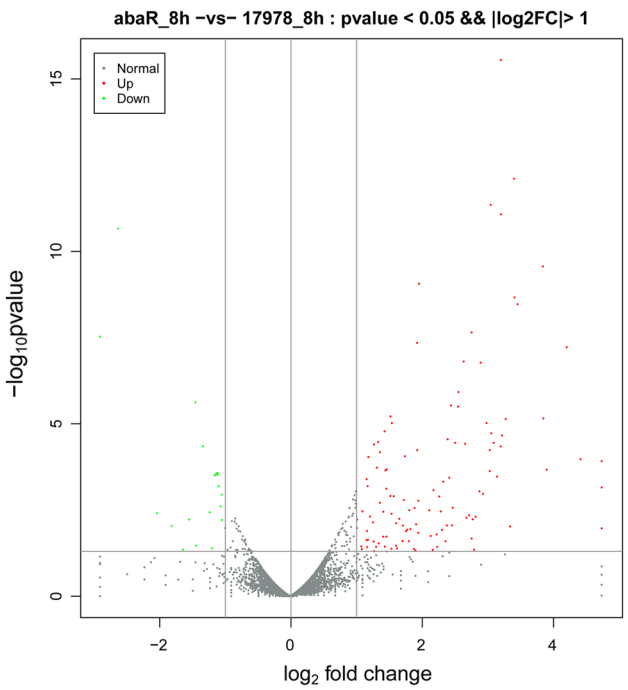

Fig. 4 Volcano plot for differentially expressed genes in *abaR* knockdown strain, compared with wide-type strain. Red spots represent genes that were significantly upregulated. Green spots represent genes that were significantly downregulated. Gray spots represent genes that were not significantly different between the two groups (Color figure online)

RT-PCR Detection

The relative expression levels of four significantly up-regulated DEGs and four significantly down-regulated DEGs were detected by PT-PCR between wild-type ATCC17978 strains and *abaR* knockdown strains (Fig. 5). As we predicted, compared in the wild-type ATCC17978 strains, the relative expression of A1S_3544, A1S_0849, A1S_3867, and A1S_3011 showed a significantly higher levels in the *abaR* knockdown strains ($P < 0.001$). The expression levels of A1S_3661, A1S_1709, A1S_2237, and A1S_2457 were significantly higher in the wild-type ATCC17978 strains than that in the *abaR* knockdown strains ($P < 0.001$).

We also detected the relative expression of A1S_0849 and A1S_2237 between wild-type ATCC17978 strains, *abaR* knockdown strains, and complementary strains (Fig. 6). The results revealed that there were no significant difference between ATCC17978 strains and complementary strains in the A1S_0849 and A1S_2237 expression. This indicates that our complementation experiment successfully restored gene expression to the wild-type level.

Discussion

A. baumannii has emerged as an important nosocomial pathogen mainly affecting patients with impaired host defences [27, pp. 640–645]. Now, *A. baumannii* is one of the most prevalent pathogens in burn-induced infections because of its multidrug-resistance, which can even induce bloodstream infections. *A. baumannii* is responsible for a vast array of infections, of which ventilator-associated pneumonia and bloodstream infections are the most common, and mortality rates can reach 35% [28, pp. 292–301]. Multidrug resistance may complicate the treatment of serious infections. Biofilm-forming ability has been found to be the major factor affecting drug resistance by *A. baumannii* [29, pp. 626–633]. Many gram-negative pathogens control their virulence through a quorum sensing (QS) system [30, p. 163]. *AbaR* is one of the QS-related genes, which is reported to play a regulatory role in biofilm formation [31, pp. 15–27]. In this study, we aimed to explore the mechanism underlying the role of *abaR* in *A. baumannii* biofilm formation.

We first determined the regulatory role of *abaR* in *A. baumannii* biofilm formation by gene knockout. In *A. baumannii,* abaR- and abaI-mediated QS plays a regulatory role in biofilm formation and surface motility [32, pp. 1719–1728]. The *abaR* gene at a size of 717 bp is localized at 1255 bp of the downstream of *abaI* gene. Additionally, we constructed an *abaR* gene knockout model in neurons using homologous recombination method. After *abaR* gene knockdown, the alternative target fragment in ATCC 17978 was determined to be 3300 bp using PCR analysis, which was similar to the

Table 1 The top 15 significant GO term and pathways of differentially expressed genes

ID	Term	Category	*P* value	Adj. *P*	Gene
GO function enrichment analysis					
GO:0009027	Tartrate dehydrogenase activity	Molecular_function	0	0	A1S_0849
GO:0046553	D-Malate dehydrogenase (decarboxylating) activity	Molecular_function	0	0	A1S_0849
GO:0019028	Viral capsid	Cellular_component	0	0	A1S_1589; A1S_2022
GO:0046797	Viral procapsid maturation	Biological_process	0	0	A1S_1590
GO:0016624	Oxidoreductase activity, acting on the aldehyde or oxo group of donors, disulfide as acceptor	Molecular_function	0	0	A1S_1699
GO:0003886	DNA(cytosine-5-)-methyltransferase activity	Molecular_function	3.84E-06	3.37E-05	A1S_1146; A1S_2036
GO:0099001	Viral genome ejection through host cell envelope, long flexible tail mechanism	Biological_process	3.84E-06	3.37E-05	A1S_1589; A1S_2022
GO:0045150	Acetoin catabolic process	Biological_process	3.84E-06	3.37E-05	A1S_1699; A1S_1700
GO:0004148	Dihydrolipoyl dehydrogenase activity	Molecular_function	3.84E-06	3.37E-05	A1S_1702; A1S_1703
GO:0009307	DNA restriction-modification system	Biological_process	1.52E-05	0.000109	A1S_1146; A1S_2036
GO:0019012	Virion	Cellular_component	1.52E-05	0.000109	A1S_1590; A1S_1595
GO:0006096	Glycolytic process	Biological_process	3.67E-05	0.000241	A1S_1701; A1S_1702; A1S_1703
GO:0015103	Inorganic anion transmembrane transporter activity	Molecular_function	0.000251	0.000903	A1S_0669
GO:0003862	3-isopropylmalate dehydrogenase activity	Molecular_function	0.000251	0.000903	A1S_0849
GO:0003992	N2-Acetyl-L-Ornithine:2-oxoglutarate 5-aminotransferase activity	Molecular_function	0.000251	0.000903	A1S_1092
Pathway enrichment analysis					
ko00010	Glycolysis/Gluconeogenesis		1.95E-08	5.06E-07	A1S_1699; A1S_1700; A1S_1701; A1S_1702; A1S_1703; A1S_2148
ko00620	Pyruvate metabolism		4.47E-07	5.82E-06	A1S_1699; A1S_1700; A1S_1701; A1S_1702; A1S_1703; A1S_2148
ko00020	Citrate cycle (TCA cycle)		1.43E-06	1.24E-05	A1S_1699; A1S_1700; A1S_1701; A1S_1702; A1S_1703
ko04922	Glucagon signaling pathway		2.43E-06	1.58E-05	A1S_1699; A1S_1700
ko01200	Carbon metabolism		1.49E-05	7.74E-05	A1S_1386; A1S_1699; A1S_1700; A1S_1701; A1S_1702; A1S_1703; A1S_2148
ko04066	HIF-1 signaling pathway		2.39E-05	0.000104	A1S_1699; A1S_1700
ko00630	Glyoxylate and dicarboxylate metabolism		0.0001	0.000373	A1S_0849; A1S_1386; A1S_1702; A1S_1703
ko00280	Valine, leucine, and isoleucine degradation		0.000298	0.000967	A1S_1376; A1S_1702; A1S_1703
ko00785	Lipoic acid metabolism		0.000578	0.00167	A1S_1698
ko00640	Propanoate metabolism		0.00101	0.002625	A1S_1702; A1S_1703; A1S_2148
ko04011	MAPK signaling pathway—yeast		0.001147	0.00271	A1S_1386
ko04211	Longevity regulating pathway		0.001895	0.004106	A1S_1386
ko04068	FoxO signaling pathway		0.002819	0.005638	A1S_1386
ko04213	Longevity regulating pathway—multiple species		0.003914	0.007268	A1S_1386
ko04212	Longevity regulating pathway—worm		0.006598	0.011436	A1S_1386

size of ΔabaR::Kn target fragment, suggesting that the *abaR* gene was successfully knocked out.

Data of the growth curve analysis showed that after 4 h of culture, the growth of the wild-type ATCC 17978 entered the exponential growth phase and entered the plateau phase at 14 h after culture. The *abaR* knockdown strain showed a similar growth curve, which indicates that no significant

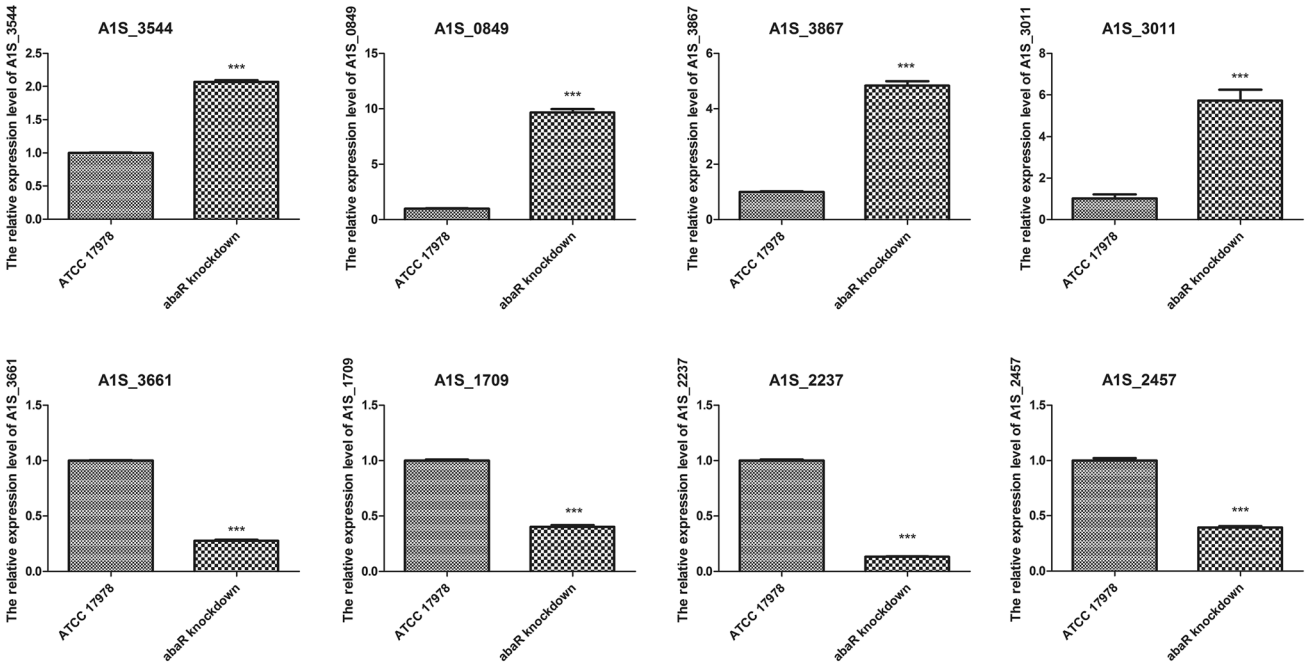

Fig. 5 Relative expression of genes in wide-type ATCC 17978 strains and *abaR* gene knockdown strains. ***$P < 0.001$, compared with wide-type ATCC 17978 strain. There were three repeats in each group. Error bar represents SD

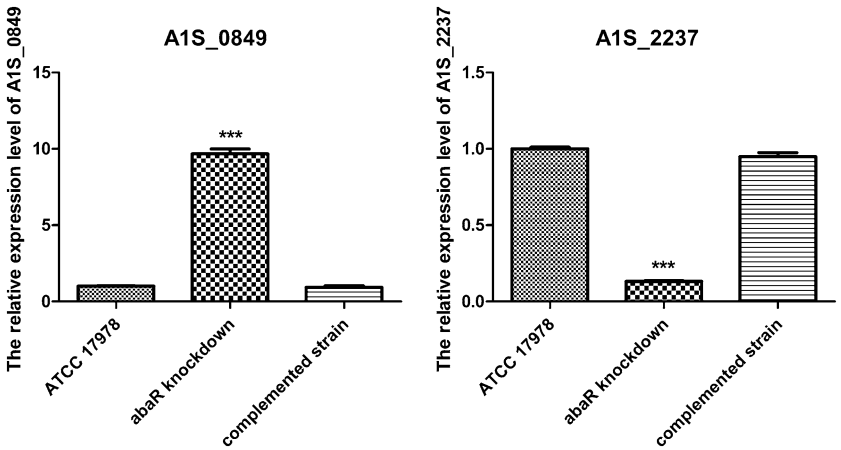

Fig. 6 Relative expression of genes in wide-type ATCC 17978 strains, *abaR* gene knockdown strains, and complemented strains. ***$P < 0.001$, compared with wide-type ATCC 17978 strain. There were three repeats in each group. Error bar represents SD

effect was observed in the growth of ATCC 17978 strain following *abaR* knockdown.

A previous study suggested that the absorbance value of drug-resistant *A. baumannii* strain was similar to sensitive strains at all culture time points. Compared with the controls, the biofilm-forming ability of the ATCC 17978 strain exposed to *N*-Heptanoyl-L-Homoserine lactone significantly declined at 12 h of culture and that of strains exposed to *N*-(3-Hydroxydodecanoyl)-DL-Homoserine lactone noticeably increased [18, pp. 200–205]. Therefore, inhibition or activation of the *abaR* gene can influence biofilm formation. Our data showed that biofilm-forming ability significantly increased in the wild-type ATCC 17978 strain compared with the *abaR* knockdown ATCC 17978 strain at 8 h of culture, which was consistent with the previous findings. All these results suggest that *abaR* knockdown affected the biofilm-forming ability of *A. baumannii* without influencing strain growth.

In addition, the mechanism of the declined biofilm-forming ability of *A. baumannii* induced by *abaR* knockdown has not been clarified completely. Thus, we performed transcriptome sequencing to identify the changed gene expression profile caused by *abaR* knockdown. Based on the results, a total of 137 genes were differentially expressed between the wild type and *abaR* knockdown strains. GO analysis showed that viral procapsid maturation was closely related to the

dysregulated expressed genes induced by *abaR* knockdown. It is reported that viral procapsid maturation is a dynamic process for viral infection [33, pp. 423–439]. The virus capsid assembly and DNA packaging have been proposed to be the target for antiviral therapy [34]. Thus, biofilm formation may share a similar group of involved genes with viral procapsid maturation and biofilm formation may be suggested as the target for antimicrobial treatment.

A previous study suggested that the changes in gene expression were more obvious in the early stage of biofilm formation than the later stages. In our study, biofilm formation was significantly changed at 8 and 24 h of culture in *abaR* knockdown strains compared with the wild-type strains. Thus, we performed transcriptome sequencing for the strains cultured for 8 h. Previous evidence showed that carbohydrate and amino acid metabolism were the necessary pathways in biofilm formation [35, 36, p. 13160]. Our study suggested that the DEGs in *abaR* knockdown strains, compared with the wild-type ATCC 17978, were significantly enriched in carbon metabolism and valine, leucine, and isoleucine degradation, which is consistent with previous reports and indicates that our findings are significant. Additionally, glycolysis and gluconeogenesis were the most significant pathways involved in the differentially expressed genes. A recent study reported that genes that play a regulatory role in gluconeogenesis are significantly upregulated in biofilm cells compared with free cells [37, p. 139]. It is reported that carbohydrates are the major composition of biofilms [38]. Carbon sources play a necessary role in the survival, growth, and infection of strains [39, pp. 2034–2045]. Accumulating evidence shows that *Candida albicans* can utilize glycolysis and gluconeogenesis alternatively for energy production [40]. Glycolysis plays a necessary role in the morphogenesis and virulence of *Candida* species. The evidence for the significant role of glycolysis and gluconeogenesis pathways in *A. Baumannii* virulence has been rarely reported. Thus, we suspect that the dysregulation of the glycolysis and gluconeogenesis pathways was induced by *abaR* knockdown in *A. Baumannii.*

Conclusion

Although this study lacks certain mechanism experiments, our verification of DEGs through RT-PCR showed that our bioinformatics analysis has a certain degree of credibility. Of course, further research on the protein level of these DEGs is also necessary in the future. In summary, *abaR* knockdown significantly decreased the biofilm-forming ability of the *A. baumannii* ATCC 17978 strain without affecting its growth. Carbon metabolism-related pathways, especially the glycolysis and gluconeogenesis pathways, were significantly dysregulated by *abaR* knockdown in *A. Baumannii.*

Supplementary Information The online version contains supplementary material available at https://doi.org/10.1007/s00284-021-02654-y.

Author Contributions Conception and design of the research: JX and XS; acquisition of data: JX and XS; analysis and interpretation of data: JX and XS; statistical analysis: JX and XS; obtaining funding: JX; drafting the manuscript: XS; revision of manuscript for important intellectual content: JX. All authors read and approved the final manuscript.

Data Availability The data used to support the findings of this study are available from the corresponding author upon request.

Code Availability Not applicable.

Declarations

Conflict of interest The authors declare that they have no conflicts of interest.

Ethical Approval Not applicable.

Consent to Participate Not applicable.

Consent for Publication Not applicable.

References

1. Dijkshoorn L, Nemec A, Seifert H (2007) An increasing threat in hospitals: multidrug-resistant *Acinetobacter baumannii*. Nat Rev Microbiol 5:939–951
2. Hu F, Zhu D, Wang F et al (2018) Current status and trends of antibacterial resistance in China. Clin Infect Dis 67:S128–S134
3. Joshi SG, Litake GM (2013) *Acinetobacter baumannii*: an emerging pathogenic threat to public health. World J Clin Infect Dis 3:25–36
4. Vázquez-López R, Solano-Gálvez SG, Juárez Vignon-Whaley JJ (2020) *Acinetobacter baumannii* resistance: a real challenge for clinicians. Antibiotics (Basel) 9:205
5. Guo H, Qin J, Xiang J (2016) Surveillance for and susceptibility of *Acinetobacter baumannii* in a large hospital and burn center in Shanghai, China, 2007–2013. Am J Infect Control 44:1718–1719
6. Trebosc V, Gartenmann S, Tötzl M et al (2019) Dissecting colistin resistance mechanisms in extensively drug-resistant *Acinetobacter baumannii* clinical isolates. mBio. https://doi.org/10.1128/mBio.01083-19
7. Yang CH, Su PW, Moi SH et al (2019) Biofilm formation in acinetobacter baumannii: genotype-phenotype correlation. Molecules (Basel, Switzerland) 24:1849
8. Longo F, Vuotto C, Donelli G (2014) Biofilm formation in *Acinetobacter baumannii*. New Microbiol 37:119–127
9. Martí S, Rodríguez-Baño J, Catel-Ferreira M et al (2011) Biofilm formation at the solid-liquid and air-liquid interfaces by *Acinetobacter* species. BMC Res Notes 4:1–4
10. Shenkutie AM, Yao MZ, Siu GK-h et al (2020) Biofilm-induced antibiotic resistance in clinical *Acinetobacter baumannii* isolates. Antibiotics 9:817
11. Flynn PB, Graham WG, Gilmore BF (2019) *Acinetobacter baumannii* biofilm biomass mediates tolerance to cold plasma. Lett Appl Microbiol 68:344–349
12. Tomaras AP, Dorsey CW, Edelmann RE et al (2003) Attachment to and biofilm formation on abiotic surfaces by *Acinetobacter*

baumannii: involvement of a novel chaperone-usher pili assembly system. Microbiology (Reading, England) 149:3473–3484
13. Loehfelm TW, Luke NR, Campagnari AA (2008) Identification and characterization of an *Acinetobacter baumannii* biofilm-associated protein. J Bacteriol 190:1036–1044
14. Piperaki ET, Tzouvelekis LS, Miriagou V et al (2019) Carbapenem-resistant *Acinetobacter baumannii*: in pursuit of an effective treatment. Clin Microbiol Infect 25:951–957
15. He X, Lu F, Yuan F et al (2015) Biofilm formation caused by clinical *Acinetobacter baumannii* isolates is associated with overexpression of the AdeFGH efflux pump. Antimicrob Agents Chemother 59:4817–4825
16. Gaddy JA, Tomaras AP, Actis LA (2009) The *Acinetobacter baumannii* 19606 OmpA protein plays a role in biofilm formation on abiotic surfaces and in the interaction of this pathogen with eukaryotic cells. Infect Immun 77:3150–3160
17. Chow JY, Yang Y, Tay SB et al (2014) Disruption of biofilm formation by the human pathogen *Acinetobacter baumannii* using engineered quorum-quenching lactonases. Antimicrob Agents Chemother 58:1802–1805
18. Guo HN, Xiang J (2017) Influences of abaR gene on biofilm formation of *Acinetobacter baumannii*. Zhonghua Shao Shang Za Zhi 33:200–205. https://doi.org/10.3760/cma.j.issn.1009-2587.2017.04.003
19. Oh MH, Han K (2020) AbaR is a LuxR type regulator essential for motility and the formation of biofilm and pellicle in *Acinetobacter baumannii*. Genes Genomics 42:1339–1346
20. Arroyo LA, Herrera CM, Fernandez L et al (2011) The pmrCAB operon mediates polymyxin resistance in *Acinetobacter baumannii* ATCC 17978 and clinical isolates through phosphoethanolamine modification of lipid A. Antimicrob Agents Chemother 55:3743–3751
21. Chhetri G, Pandey T, Chinta R et al (2015) An improved method for high-level soluble expression and purification of recombinant amyloid-beta peptide for in vitro studies. Protein Expr Purif 114:71–76. https://doi.org/10.1016/j.pep.2015.05.015
22. Du P, Liu D, Song H et al (2020) Novel IS26-mediated hybrid plasmid harbouring tet(X4) in *Escherichia coli*. J Global Antimicrobial Resistance 21:162–168
23. Rumbo-Feal S, Gómez MJ, Gayoso C et al (2013) Whole transcriptome analysis of *Acinetobacter baumannii* assessed by RNA-sequencing reveals different mRNA expression profiles in biofilm compared to planktonic cells. PLoS ONE 8:e72968
24. Culviner PH, Guegler CK, Laub MT (2020) A simple, cost-effective, and robust method for rRNA depletion in RNA-sequencing studies. mBio. https://doi.org/10.1128/mBio.00010-20
25. Consortium GO (2006) The gene ontology (GO) project in 2006. Nucleic Acids Res 34:D322–D326
26. Kanehisa M (2002) The KEGG database. Novartis Foundation Symposium. Wiley, Hoboken, pp 91–100
27. Hu Y-F, Hou CJ-Y, Kuo C-F et al (2017) Emergence of carbapenem-resistant *Acinetobacter baumannii* ST787 in clinical isolates from blood in a tertiary teaching hospital in Northern Taiwan. J Microbiol Immunol Infect 50:640–5
28. Antunes LC, Visca P, Towner KJ (2014) *Acinetobacter baumannii*: evolution of a global pathogen. Pathogens Dis 71:292–301
29. Nor A'shimi MH, Alattraqchi AG, Mohd Rani F et al (2019) Biocide susceptibilities and biofilm-forming capacities of *Acinetobacter baumannii* clinical isolates from Malaysia. J Infect Dev Ctries 13:626–33
30. Vadakkan K, Vijayanand S, Hemapriya J et al (2019) Quorum sensing inimical activity of *Tribulus terrestris* against gram negative bacterial pathogens by signalling interference. 3 Biotech 9:163
31. Saipriya K, Swathi CH, Ratnakar KS et al (2020) Quorum-sensing system in *Acinetobacter baumannii*: a potential target for new drug development. J Appl Microbiol 128:15–27. https://doi.org/10.1111/jam.14330
32. Stacy DM, Welsh MA, Rather PN et al (2012) Attenuation of quorum sensing in the pathogen *Acinetobacter baumannii* using non-native N-Acyl homoserine lactones. ACS Chem Biol 7:1719–1728
33. Cardone G, Heymann JB, Cheng N et al (2012) Procapsid assembly, maturation, nuclear exit: dynamic steps in the production of infectious herpesvirions. In: Rossmann MG, Rao VB (eds) Viral molecular machines. Springer, Boston, pp 423–439
34. Zhang X, Jia R, Zhou J et al (2016) Capsid-targeted viral inactivation: a novel tactic for inhibiting replication in viral infections. Viruses 8:258
35. Lemos JA, Palmer SR, Zeng L et al (2019) The biology of *Streptococcus mutans*. Microbiol Spectr 7(1):1–26. https://doi.org/10.1128/microbiolspec.GPP3-0051-2018
36. Lu H, Que Y, Wu X et al (2019) Metabolomics deciphered metabolic reprogramming required for biofilm formation. Sci Rep 9:13160–13166
37. Li Z, Chen Y, Liu D et al (2015) Involvement of glycolysis/gluconeogenesis and signaling regulatory pathways in *Saccharomyces cerevisiae* biofilms during fermentation. Front Microbiol 6:139
38. Jara J, Alarcón F, Monnappa AK et al (2021) Self-adaptation of pseudomonas fluorescens biofilms to hydrodynamic stress. Front Microbiol. https://doi.org/10.3389/fmicb.2020.588884
39. Carlson HK, Lui LM, Price MN et al (2020) Selective carbon sources influence the end products of microbial nitrate respiration. ISME J 14:2034–2045
40. Sandai D, Tabana YM, Ouweini AE et al (2016) Resistance of *Candida albicans* biofilms to drugs and the host immune system. Jundishapur J Microbiol. https://doi.org/10.5812/jjm.37385